Dynamics of a self-propelled particle under different driving modes in a channel flow*

Zhenyu Ouyang(欧阳振宇), Jianzhong Lin(林建忠)†, and Xiaoke Ku(库晓珂)

State Key Laboratory of Fluid Power and Mechatronic Systems, Zhejiang University, Hangzhou 310027, *China*

(Received 6 May 2016; revised manuscript received 28 August 2016; published online 29 November 2016)

In this paper, a model that combines the lattice Boltzmann method with the singularity distribution method is proposed to simulate a self-propelled particle swimming (exhibiting translation and rotation) in a channel flow. The results show that the velocity distribution for a self-propelled particle swimming deviates from a Maxwellian distribution and exhibits high-velocity tails. The influence of an eccentric potential doublet on the translation velocity of the particle is significant. The velocity decay process can be described using a double exponential model form. No large differences in the velocity distribution were observed for different translation Reynolds numbers, rotation Reynolds numbers, or regular intervals.

Keywords: lattice Boltzmann method, singularity distribution method, self-propelled particle, driving modes

PACS: 05.20.Dd, 47.11.Qr, 47.57.E– **DOI:** 10.1088/1674-1056/26/1/014701

1. Introduction

Self-propelled particle swimming has gained wide attention due to its relevance to biological and technological applications. Micro-swimmers may use various driving mechanisms, such as flagellar propulsion,[1–3] beating cilia,[3] surface distortions,[4] chemical reactions,[5,6] or actin-tail polymerisation.[7,8] Although notable differences between these mechanisms exist, the universality in hydrodynamic behaviour is obvious. For many biologically relevant systems, it is typical that self-propulsive swimming contributes to non-equilibrium dynamics systems.[9,10] The experimental observation that swimming particles enhance hydrodynamic diffusion has been confirmed by numerical simulations.[11,12] The presence of swimming particles always affects the stability of suspensions.[13,14] On the other hand, the rheological characteristics of suspensions that result from swimming particles may play a major role in channel flow. Bioconvection can occur when swimmers share a mean upward movement because of the effects of gravitational torque, chemotaxis, or phototaxis.[15] Therefore, investigation of the motion characteristics and effects of self-propelled swimmers on the properties of fluid media is important to understanding the transformation mechanism of biological system energy and improving the design of micro bionic robots.

Most of the research on the motion of self-propelled particles suspended in Newtonian fluids have employed analytical solutions or numerical methods to examine motion under the condition of low-Reynolds-number flow. From a microscopic perspective, Lighthill[16] first proposed the model of a squirmer, which has a spherical shape with surface tangential velocities, based on a solution of the Stokes equation in a spherical coordinate system. Blake[17] later extended this model to the dynamics of ciliary propulsion of a microscopic organism. Magar *et al.*[18] developed a model for nutrition uptake by a self-propelled steady squirmer. Recently, Ishikawa *et al.*[19] developed a database for an interacting pair of squirmers from which one can easily predict the motion of self-propulsion suspensions using a boundary element method. They used the interaction model to study the rheology of a semi-dilute suspension of bottom-heavy and non-bottom-heavy squirmers[20] and the diffusion of swimming micro-organisms in a semi-dilute suspension.[21] They also studied the orientation order in a concentrated suspension of spherical microswimmers.[22] This squirmer model is an accurate combination of an analytical solution and a boundary element method which is precise in dealing with a complex boundary and near-wall flow. However, this method requires a number of integrals and even a singular integral, which requires huge computing resources. Taking into consideration the interaction between particles, Hernández-Ortiz *et al.* proposed a model in which a force dipole is drawn into a fluid to describe the effects of self-propelled particles.[13,23] Saintillan and Shelley[24] proposed a model based on the slender-body theory in which swimming particles are regarded as self-propelled rigid slender rods that impose a given shear stress on the surrounding fluid. These models seek to describe the movement mechanism of self-propelled particles and how they affect the characteristics of the surrounding fluid.

The lattice Boltzmann method (LBM), which is widely used in the simulation of various types of flow,[25–29] relies on the fact that the macroscopic dynamics of fluid flow does not depend on the microscopic details of the fluid field. The LBM was first proposed by Ladd *et al.* to simulate passive sus-

*Project supported by the National Natural Science Foundation of China (Grant No. 11632016).

†Corresponding author. E-mail: mecjzlin@public.zju.edu.cn

© 2017 Chinese Physical Society and IOP Publishing Ltd

pensions at finite Reynolds numbers.[30–32] Aidun *et al.*[33–35] developed this method and added 'virtual nodes' to the solid boundaries to simulate passive particles near contact. Recently, Ramachandran *et al.*[36] proposed an LBM model for active suspensions, in which two types of particles (movers and shakers) are defined by different distributions for point forces as a force dipole and a D2Q7 LBM model is used to simulate individual and multiple self-propelled colloidal particles. The researchers found that the velocity of the mover was directly proportional to the asymmetry of the position of the force distribution and that the statistical properties of the velocity field generated by the activity deviated from those of equilibrium fluids. Alarcón and Pagonabarraga[37] proposed a three-dimensional LBM for suspensions of self-propelled particles using a squirmer model in which the appropriate boundary conditions for the Stokes equation at the surfaces of spherical particles were imposed to induce a slip velocity between the fluid and the particles. They employed this method to characterise the hydrodynamic stresses induced by active swimmers, and they found that active stresses played a dominant role in decorrelating the collective motion of squirmers and that contractile squirmers formed significant aggregates.

Several numerical studies have been performed in the past few years to explore the mechanism of self-propulsive particle movement using the lattice Boltzmann method, in which a force dipole or a slip velocity is exerted on the boundaries of the particles as the driving mode. However, it is difficult to apply this approach to particles with irregular geometric shapes. Chwang and Wu[38–40] proposed a singularity distribution method, based on the theory for low-Reynolds-number flows, with which the real movement characteristics of self-propelled particles with complicated boundaries can be simulated. The Stokes flow around an object with arbitrary shapes can be simulated by properly adjusting the type, position, and intensity of fundamental Stokes flow singularities in the interior of an object using the singularity distribution method. In this paper, we present a model that combines the lattice Boltzmann method with the singularity distribution method to simulate a self-propulsive particle swimming in a channel flow. The behaviours of self-propelled particles' translation, rotation, period of transition between translation and rotation, and decay of the particle velocity were analysed.

2. Numerical methods

2.1. Lattice Boltzmann scheme

The LBM is different from schemes based on the continuum assumption of fluids. In the LBM, the discrete microscopic velocity space is given as follows:[41]

$$f_i(\boldsymbol{x}+\boldsymbol{e}_i,t+1)-f_i(\boldsymbol{x},t)=\Omega_i, \tag{1}$$

where f_i is the density distribution function; $\boldsymbol{e}_i$ is the streaming velocity in the ith direction in the phase space; $i=0,1,\ldots,N$; Ω_i is the collision operator; and the Bhatnagar–Gross–Krook (BGK) collision term is given as follows:[42]

$$\Omega_i=-\frac{1}{\tau}(f_i-f_i^{\mathrm{eq}}), \tag{2}$$

where f_i^{eq} is the local equilibrium distribution, τ is the single relaxation time. For a square or cubic lattice, the equilibrium function f_i^{eq} is as follows:[43]

$$f_i^{\mathrm{eq}}=\rho\omega_i\left[1+\frac{3}{c^2}\boldsymbol{e}_i\cdot\boldsymbol{u}+\frac{9}{2c^4}(\boldsymbol{e}_i\cdot\boldsymbol{u})^2-\frac{3\boldsymbol{u}^2}{2c^2}\right],\ i=0,\ldots,N, \tag{3}$$

where ρ and $\boldsymbol{u}$ are the macroscopic fluid density and velocity, respectively:

$$\rho=\sum_i f_i,\quad \boldsymbol{u}=\frac{1}{\rho}\sum_i f_i\boldsymbol{e}_i. \tag{4}$$

In the nine-bit LBGK model, the two-dimensional velocity in the phase space is discretised in nine directions:

$$\boldsymbol{e}_0=0;\ \ \boldsymbol{e}_i=\{\cos[\pi(i-1)/2],\ \sin[\pi(i-1)/2]\},\ \ i=1-4,$$
$$\boldsymbol{e}_i=\sqrt{2}\{\cos[\pi(i-4.5)/2],\ \sin[\pi(i-4.5)/2]\},\ \ i=5-8.$$

The kinematic viscosity for the nine-speed model is $\upsilon=c^2\Delta t(\tau-0.5)/3$, and $c=\Delta x/\Delta t$ is the lattice speed. In Eq. (3), ω_i is equal to 4/9 for $i=$ 1–4 and 1/36 for $i=$ 5–8.

Within the limit of long wavelengths, the lattice Boltzmann equation recovers the following quasi-incompressible Navier–Stokes equation by the Chapman–Enskog multi-scaling expansion:[44]

$$\frac{\partial\rho}{\partial t}+\nabla\cdot\rho\boldsymbol{u}=0, \tag{5}$$

$$\frac{\partial\rho\boldsymbol{u}}{\partial t}+\nabla\cdot\rho\boldsymbol{u}\boldsymbol{u}=-\nabla P+\mu\Delta\boldsymbol{u}, \tag{6}$$

where $P=\rho c_{\mathrm{s}}^2$ is the fluid pressure, c_{s} is the sound speed with $c_{\mathrm{s}}^2=c^2/3$, and $\mu=\rho\upsilon$ is the dynamic viscosity.

Ladd[31,32] and Aidun *et al.*[34] used the momentum exchange method to propose a modified bounce-back rule for a moving wall. If we place the boundary nodes on the links connecting the interior and exterior nodes,

$$f_{i'}(\boldsymbol{x},t+1)=f_i(\boldsymbol{x},t_+)-2B_i(\boldsymbol{e}_i\cdot\boldsymbol{u}_{\mathrm{b}}), \tag{7}$$

where t_+ denotes the post-collision time; i is the incident direction; i' is the reflected direction; $B_i=3\rho\omega_i/c^2$; $\boldsymbol{u}_{\mathrm{b}}$ is the velocity at the particle surface; $\boldsymbol{u}_{\mathrm{b}}=\boldsymbol{u}_0+\boldsymbol{\Omega}\times\boldsymbol{x}_{\mathrm{b}}$, where $\boldsymbol{u}_0$ is the translational velocity of the mass centre of the particle; $\boldsymbol{\Omega}$ is the angular velocity of the particle; and $\boldsymbol{x}_{\mathrm{b}}=\boldsymbol{x}+\boldsymbol{e}_i/2-\boldsymbol{x}_0$, where $\boldsymbol{x}_0$ is the position of the mass centre. The force and torque exerted by the fluid at $\boldsymbol{x}_{\mathrm{b}}$ are given by the following equations:

$$\boldsymbol{F}\left(\boldsymbol{x}+\frac{1}{2}\boldsymbol{e}_i,t+\frac{1}{2}\right)=2\boldsymbol{e}_i[f_i(\boldsymbol{x},t_+)-B_i(\boldsymbol{e}_i\cdot\boldsymbol{u}_{\mathrm{b}})], \tag{8}$$

$$\boldsymbol{T}\left(\boldsymbol{x}+\frac{1}{2}\boldsymbol{e}_i,t+\frac{1}{2}\right)=\boldsymbol{x}_{\mathrm{b}}\times\boldsymbol{F}. \tag{9}$$

2.2. Self-propulsion model

For the case in which the inertial effects are negligible in comparison to the viscous forces, under the condition of low-Reynolds-number flow, the Navier–Stokes equations are usually simplified to the Stokes equations

$$\nabla \cdot \boldsymbol{u} = 0, \tag{10a}$$

$$\nabla P = \mu \nabla^2 \boldsymbol{u} + \boldsymbol{f}, \tag{10b}$$

where $\boldsymbol{u}$ is the velocity vector, p is the pressure, μ is the constant viscosity coefficient, $\boldsymbol{f}(\boldsymbol{x})$ is the external force per unit volume, and $\boldsymbol{x}$ is the position vector in a three-dimensional Euclidean space. If the value of $\boldsymbol{f}(\boldsymbol{x})$ is zero and the pressure p is constant, the solutions of Eq. (10) are the same as the solutions of classical potential flow in which the velocity vector $\boldsymbol{u}$ and the velocity potential $\boldsymbol{\Phi}$ satisfy the following harmonic functions:

$$\nabla^2 \boldsymbol{\Phi} = 0, \tag{11a}$$

$$\nabla^2 \boldsymbol{u} = \boldsymbol{0}. \tag{11b}$$

We can draw the conclusion that any velocity field $\boldsymbol{u}$ of incompressible potential flow with a uniform pressure field ($p =$ a constant) is the solution of Stokes flow, which means that the two types of flows are similar in kinematics although different in dynamics. Thus, we can add $p =$ a constant to the basic solution of unbounded potential flow as the special solution of Stokes flow that we need. In the (r, θ, ϕ) spherical coordinate system, the velocity potential Φ that satisfies the Laplace equation can be solved as follows:[45]

$$\sum_{n=0}^{\infty} \sum_{m=0}^{n} \frac{1}{r^{n+1}} P_n^m(\cos\theta)[C_{nm}\cos m\phi + D_{nm}\sin m\phi], \tag{12}$$

where $P_n^m(x)$ is the first kind of associated Legendre polynomials and C_{nm}, D_{nm} are two arbitrary constants. In the formula, the $n = 0$ item $C_{00}\frac{1}{r}$ represents the velocity potential of a point source, and the $n = 1$ items,

$$C_{10}\frac{\cos\theta}{r^2} = C_{10}\frac{z}{r^3}, \tag{13a}$$

$$-C_{11}\frac{\sin\theta\cos\phi}{r^2} = -C_{11}\frac{x}{r^3}, \tag{13b}$$

$$-D_{11}\frac{\sin\theta\sin\phi}{r^2} = -D_{11}\frac{y}{r^3}, \tag{13c}$$

represent the velocity potentials of the doublet for the displacement axis in the z, x, and y directions, respectively. We can obtain the velocities of the point source u_i^Q as follows:

$$u_i^Q = \frac{Qr_i}{4\pi r^3}, \tag{14a}$$

$$p^Q = \text{constant}, \tag{14b}$$

where i is the direction of the radius vector (the point source is located at the origin of the coordinate system).

$$Q = \oiint_S \boldsymbol{u}_i^Q \cdot \boldsymbol{n}\,\mathrm{d}S, \tag{15}$$

represents the volume flux that flows out from any surface enclosing the origin, which is also called the intensity of the point source ($Q < 0$ denotes a point sink). A point source and a point sink can form a potential doublet u_i^{D}:

$$u_i^{\mathrm{D}} = \frac{-D_j}{4\pi}\left(\frac{\delta_{ij}}{r^3} - \frac{3x_i x_j}{r^5}\right), \tag{16a}$$

$$p^{\mathrm{D}} = \text{constant}, \tag{16b}$$

where D_j represents the intensity of the potential doublet for a displacement axis in the j direction. Note that we have not mentioned the other fundamental singular solutions of Stokes flow, including a Stokeslet and its derivatives, known as rotlets, stresslets, and higher-order poles derived from them. The reason is that research has shown that the fluid field driven by self-propelled particles is not like the flow of a Stokes doublet but rather more like that of a potential doublet.[46]

3. Results and discussion

3.1. Computation parameters

In the simulations, we modelled an active self-propelled particle in a typical two-dimensional static flow field, as shown in Fig. 1. The x–y coordinate system was fixed at the centre of the cylinder, with x in the channel wall direction and y in the transverse direction. No-slip and no-penetration boundary conditions were imposed on the channel wall. The particle was 10 μm in diameter (D). The deformation and bending of the particle caused by the flow were ignored, and the ratio of the particle density to that of the flow was taken to be equal to 1. The lattice spacing was 1 μm, and the time step was 1 μs. Before we began a simulation, we arranged the periodic boundary length in the flow direction from $10D$ to $40D$ to ensure that the effects of the periodic boundary conditions on the simulation of an unbound wall in the x direction would be negligible. Our results showed that, at small Reynolds numbers, the simulations were insensitive to these lengths, so we typically chose $20D$ as the periodic repeat length. A particle was situated in the cell, as shown in Fig. 1, and a velocity distribution was assigned to the fluid boundary nodes representing a specific potential doublet in the particle.

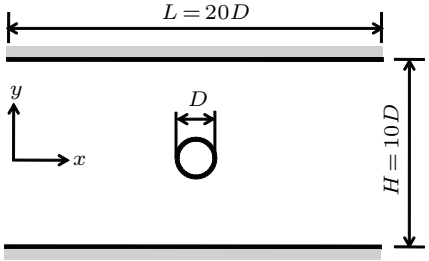


Fig. 1. Schematic illustration of the flow field and the coordinate system.

Figure 2 shows the translation and rotation of a self-propelled particle in the central part of a fluid field. The streamlines depict the two typical swimming modes that occur under low-Reynolds-number flow.

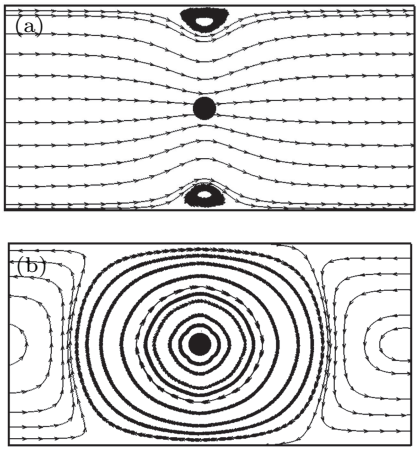


Fig. 2. Illustration of streamlines for a single self-propulsive particle swimming in the channel: (a) translation, (b) rotation.

3.2. Translation of single particle in the channel

Compared with the boundary element method that Ishikawa *et al.*[19–22] proposed for use in simulating active suspensions, the method we propose here can reduce the huge amount of computational effort required as a result of the large number of singular numerical integrations involved. The advantage of LBM is that it avoids the need to solve Poisson's equation and is easy to employ using parallel computation, which greatly reduces the computational resources required. On the other hand, unlike previously proposed computational schemes that lacked the ability to address complicated boundaries, the proposed method can construct the exact velocity distributions of particles with complex geometric shapes by arranging the basic singularities of different types of Stokes flow within a certain law. That is to say, the method we propose here possesses the advantages of both the LBM and the method of singularity distribution.

A self-propelled particle can swim continuously or at regular intervals. We call the interval between two adjacent times the switching time. We define the Reynolds number Re_{T} as a dimensionless constant associated with translational motion. Figure 3 shows the velocity distributions at different switching times. We can see that the distributions illustrate a dependence on the switching time. The different velocity distributions in the fluid depart from a continuous-swimming Maxwellian distribution in the areas of lower and higher velocities. A self-propelled particle results in a system that is out of equilibrium where energy is pumped into the fluid field, creating thicker high-velocity distribution tails. In addition, although the size of the particle is much smaller than the fluid domain, it can create thicker low-velocity distribution tails. The nearly identical low-velocity distributions with decreasing velocity are consistent with one of the Stokes flow characteristics, i.e., that the flow disturbance attenuation is slow and broadly distributed.

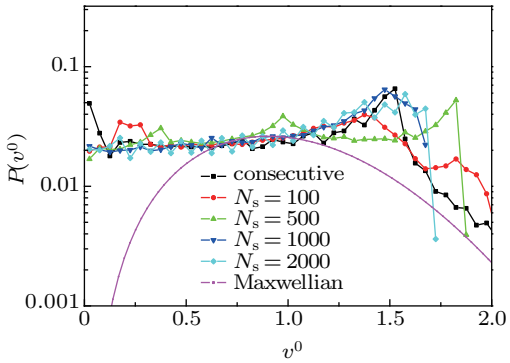


Fig. 3. (color online) Velocity distributions at different switching time. The different numbers N_{s} stand for different interval time steps, for example, the number 100 means 100 μs (100×1 μs). $Re_{\mathrm{T}} = U_{\mathrm{T}}D/\upsilon$, U_{T} is the given translational velocity of the fluid boundary node where the outer normal direction of the particle is consistent with the particle movement direction, D is the particle length scale and υ is the kinematic viscosity. For Maxwellian, $N_{\mathrm{s}} = 1000$, $Re_{\mathrm{T}} = 0.01$. v^0 is the fluid node velocities scaled by the average value of the fluid node velocities. $P(v^0)$ is the normalised fluid nodes velocity distribution.

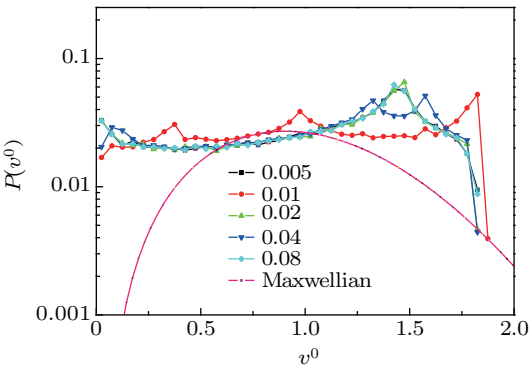


Fig. 4. (color online) Velocity distributions for different Re_{T}. For Maxwellian, $N_{\mathrm{s}} = 500$, $Re_{\mathrm{T}} = 0.02$.

The velocity distributions for the translation of a single particle at different Re_{T} values are shown in Fig. 4, which is analogous to Fig. 3.

The potential doublet at different positions along the orientation vector $\boldsymbol{e}$ and the velocity distribution of the fluid nodes at different eccentric distances are shown in Fig. 5. We can see that changes in the eccentricity have no significant effect on the velocity distribution.

The decrease in the velocity of a self-propelled particle when its activity is switched off was also studied at three Reynolds numbers. The results show that the shapes of the decay curves are consistent with a double exponential function. Figure 6 shows a fitted curve for the case of $Re_{\mathrm{T}} = 0.005$. This curve also coincides with all points at $Re_{\mathrm{T}} = 0.02$ and $Re_{\mathrm{T}} = 0.08$. The regression line is of the following form:

$$y = A_1 \times \exp(-x/t_1) + A_2 \times \exp(-x/t_2) + y_0, \qquad (17)$$

with $y_0 = 3.4563 \times 10^{-4}$, $A_1 = 0.56153$, $t_1 = 9.68898 \times 10^{-4}$, $A_2 = 2.79021$, and $t_2 = 5.76701 \times 10^{-5}$.

The timescales t_1 and t_2 stem from different dissipative mechanisms. The short timescale t_2 stems from the friction generated by relative motion between the particle boundary and the fluid, and the long timescale t_1 stems from the fluid drag force that exists before the particle becomes stationary.

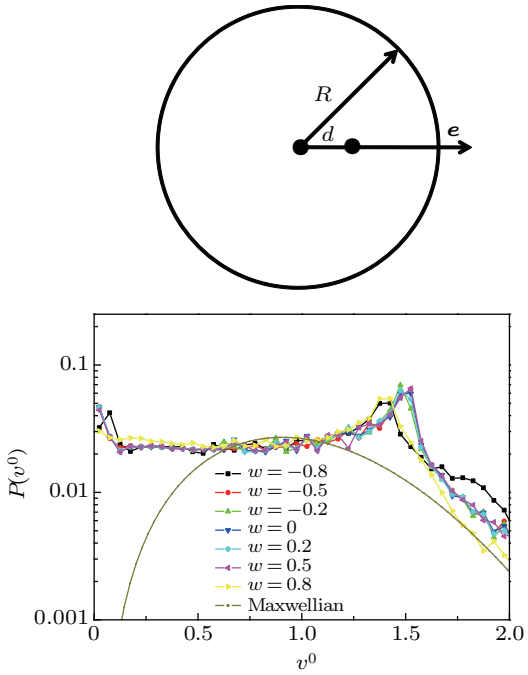


Fig. 5. (color online) Schematic illustration of a particle with eccentric potential doublet position and velocity distributions at different potential doublet eccentric distances. $w = d/R$. For Maxwellian, $w = 0$, N_s = consecutive, $Re_T = 0.01$.

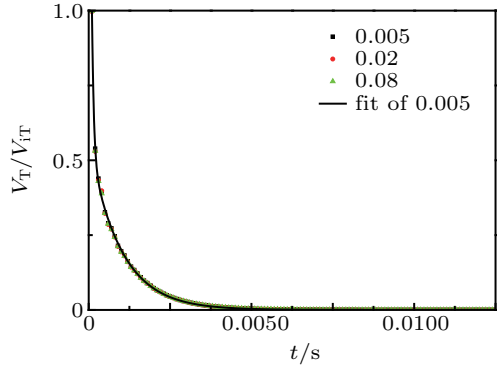


Fig. 6. (color online) Particle translational velocity decay under different Re_T with time t after the driving is switched off. V_T is the particle translational velocity, and V_{iT} is the particle translational velocity before the activity was switched off.

Different eccentric distances can also lead to a various self-propulsion velocities, even though we assigned an equal-intensity potential doublet to the particle. A fitted parabolic curve of the following form is shown in Fig. 7 for different eccentric distances:

$$y = A + B_1 x + B_2 x^2 + B_3 x^3 + B_4 x^4 + B_5 x^5 + B_6 x^6, \quad (18)$$

with $A = 5.04046 \times 10^{-4}$, $B_1 = -2.58696 \times 10^{-5}$, $B_2 = 0.00218$, $B_3 = 1.7603 \times 10^{-4}$, $B_4 = -0.00448$, $B_5 = -1.95168 \times 10^{-4}$, and $B_6 = 0.01125$.

As the figure shows, the eccentric distance can determine the self-propulsion efficiency. The farther the eccentric point is from the centre, the higher the particle velocity is.

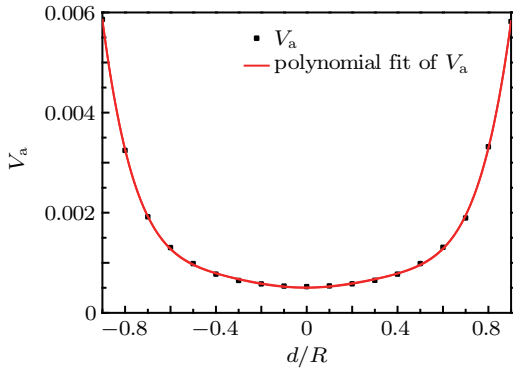


Fig. 7. (color online) The change of velocity for the single particle with different $w = d/R$, and V_a is the average velocity of the self-propulsion particle.

3.3. Rotation of single particle in the channel

To explore the characteristics of the rotation of a single self-propelled particle in a channel, we defined a rotation Reynolds number Re_R and simulated rotational motion in the flow field by assigning a rotation speed to the fluid boundary of the particle. Three nearly overlapped distribution curves for three different Re_R values are shown in Fig. 8. For $Re_R = 0.08$, there is a peak in the low-velocity region, and the curve is smooth in other regions. At very high velocities, the distribution decays so slowly as to be almost uniform when the self-propelled particle is rotating. The peak in the low-velocity region may be attributed to the effect of the boundary limitation which prevents the propagation and attenuation of fluid velocities toward further distances.

The decay process of the rotation of a single particle is different from that of its translation, in that rotation requires less time than translation. Figure 9 shows a fitted curve for the case of $Re_T = 0.005$. This curve also coincides with all points at $Re_T = 0.02$ and $Re_T = 0.08$. A double exponential curve of the following form was used to describe the decay process and is shown in Fig. 9:

$$y = y_0 + A_1 \times \exp(-(x - x_0)/t_1) + A_2 \times \exp(-(x - x_0)/t_2), \quad (19)$$

with $y_0 = 6.82982 \times 10^{-4}$, $A_1 = 1.24957$, $t_1 = 1.11146 \times 10^{-5}$, $A_2 = 0.16235$, and $t_2 = 1.07353 \times 10^{-4}$.

The short timescale t_1 and the long timescale t_2 are determined by the friction and drag force, respectively.

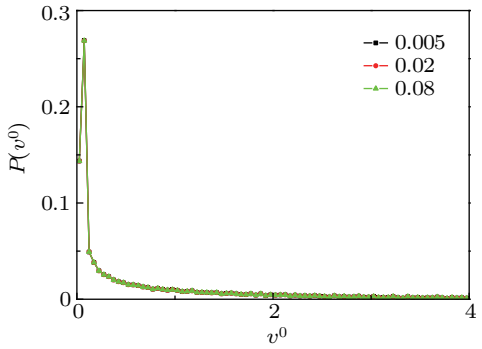


Fig. 8. (color online) Velocity distributions for different Re_R. $Re_R = U_R D/\upsilon$, U_R is the given rotation velocity of the self-propulsion particle at fluid boundary. $U_R = \omega_R D$, ω_R is the angular velocity of the particle, D is the particle length scale and υ is the kinematic viscosity. v^0 is the fluid node velocities scaled by the average value of the fluid node velocities.

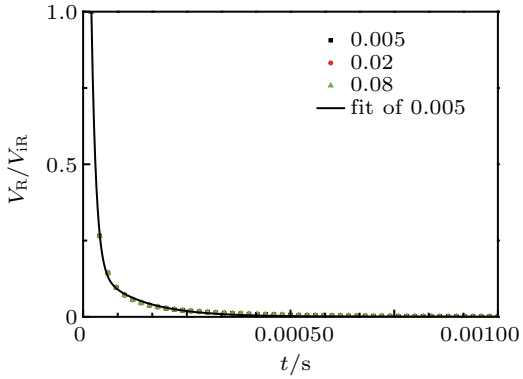


Fig. 9. (color online) Particle rotation velocity decay under different Re_R with time t after the driving is switched off. V_R is the particle rotational velocity, $V_R = \omega_R D$, ω_R is the angular velocity of the particle, D is the particle length scale. V_{iR} is the particle rotational velocity before the activity was switched off.

3.4. Translation and rotation of single particle in the channel

A self-propelled micro-organism often switches its mode of motion between translation and rotation. For example, a bacterium cell usually exhibits a run-and-tumble motion in which it changes the direction of swimming by the rotation of any motor, i.e., unravelling of flagellar bundles.[15] Thus, it makes sense to study fluid velocity distributions after the sudden movement pattern changes of a single particle. Figure 10 shows that at $Re_T = 0.01$, a particle abruptly changes its swimming direction by rotating anticlockwise to different degrees. The curves in the figure exhibit different peak velocities with increasing rotation angle. The greater the angle is, the smaller the peak velocity is, and the higher the distribution peak value is. The result is gradually upturned tails. At the beginning of an angle of $\pi/2$, the effect of the translation velocity becomes insignificant because of the sufficiently long decay time. Rotational motion thus plays a major role in the distribution of velocity.

A single particle rotating through a specific angle $\pi/4$ for various Re_T values was studied. The results are shown in Fig. 11. We can see that the velocity distributions in the high-velocity regions are coincident, but in the low-velocity region, the distributions are different. The curves shown in Figs. 10 and 11 resemble long-tailed non-Maxwellian distributions, which can be considered to be the result of the kinetic energy imparted to the fluid by the particle's activity.

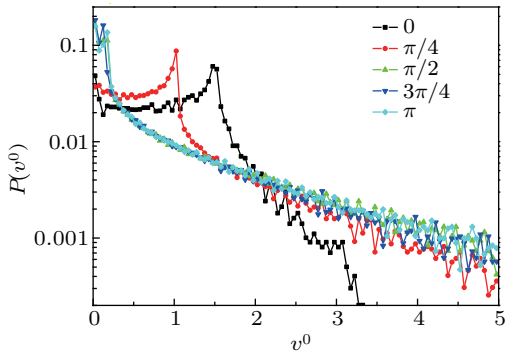


Fig. 10. (color online) Fluid node's velocity distributions for different rotation angles at $Re_T = 0.01$ and $Re_R = 0.1$.

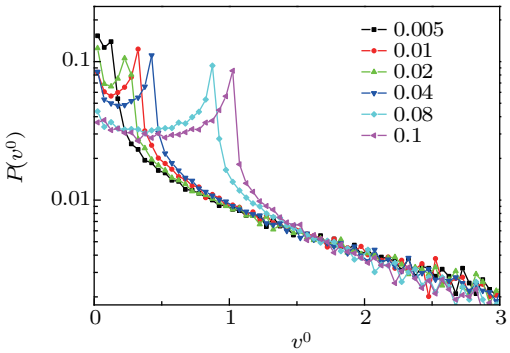


Fig. 11. (color online) Fluid node's velocity distributions for different Re_R at $Re_T = 0.01$.

4. Conclusion

A model that combines the lattice Boltzmann method with the singularity distribution method is proposed to simulate a self-propelled particle swimming (exhibiting translation and rotation) in a channel. Periodic boundary conditions were used in the simulations conducted, and the interaction between a single particle and the channel was not taken into account. The results show that the velocity distributions for translation and rotation of a single self-propelled particle deviate from a Maxwellian distribution, with high-velocity tails being observed because of the pumping of energy into the system. The effects of different potential doublet eccentricities on the translation velocity of a single self-propelled particle are significant. The double-exponential distributions decay when the swimming particle is switched off, which confirms that friction and drag force are the two major sources of resistance. The velocity distribution of a self-propelled particle is different from the Maxwellian distribution of a passive particle. No large differences in the velocity distribution were

observed for different translation Reynolds numbers, rotation Reynolds numbers, or regular intervals.

References

[1] Dreyfus R, Baudry J, Roper M L, Stone H A, Fermigier M and Bibette J 2005 *Nature* **437** 862
[2] Yu T S, Lauga E and Hosoi A E 2006 *Phys. Fluids* **18** 091701
[3] Brennen C and Winet H 1977 *Annu. Rev. Fluid Mech.* **9** 339
[4] Ajdari A and Stone H A 1999 *Phys. Fluids* **11** 1275
[5] Paxton W F, Kistler K C, Olmeda C C, Sen A, Angelo S K S, Cao Y, Mallouk T E, Lammert P E and Crespi V H 2004 *J. Am. Chem. Soc.* **126** 13424
[6] Golestanian R, Liverpool T B and Ajdari A 2005 *Phys. Rev. Lett.* **94** 220801
[7] Gouin E, Welch M D and Cossart P 2005 *Curr. Opin. Microbiol.* **8** 35
[8] Leshansky A M 2006 *Phys.Rev. E* **74** 012901
[9] Schmittmann B and Zia R K P 1995 *Statistical Mechanics of Driven Diffusive Systems, in Phase Transitions and Critical Phenomena* (New York: Academic) Vol. 17, p. 1
[10] Marchetti M C, Joanny J F, Ramaswamy S, Liverpool T B, Prost J, Rao M and Simha R S 2013 *Rev. Mod. Phys.* **85** 1143
[11] Wu X L and Libchaber A 2000 *Phys. Rev. Lett.* **84** 3017
[12] Kim M J and Breuer K S 2004 *Phys. Fluids* **16** L78
[13] Hernández-Ortiz J P, Stoltz C G and Graham M D 2005 *Phys. Rev. Lett.* **95** 204501
[14] Underhill P T, Hernández-Ortiz J P and Graham M D 2008 *Phys. Rev. Lett.* **100** 248101
[15] Donald L Koch and Ganesh S 2011 *Annu. Rev. Fluid Mech.* **43** 637
[16] Lighthill M J 1952 *Comm. Pure Appl. Math.* **5** 1091
[17] Blake J R 1971 *J. Fluid Mech.* **46** 199
[18] Magar V, Goto T and Pedley T J 2003 *J. Mech. Appl. Maths.* **56** 65
[19] Ishikawa T, Simmonds M P and Pedley T J 2006 *J. Fluid Mech.* **568** 119
[20] Ishikawa T and Pedley T J 2007 *J. Fluid Mech.* **588** 399
[21] Ishikawa T and Pedley T J 2007 *J. Fluid Mech.* **588** 437
[22] Evans A A, Ishikawa T, Yamaguchi T and Lauga E 2011 *Phys. Fluids* **23** 111702
[23] Underhill P T, Hernández-Ortiz J P and Graham M D 2008 *Phys. Rev. Lett.* **100** 248101
[24] Saintillan D and Shelley M J 2007 *Phys. Rev. Lett.* **99** 058102
[25] Zhang T, Shi B C and Chai Z H 2015 *Acta Phys. Sin.* **64** 154701 (in Chinese)
[26] Nie D M and Lin J Z 2010 *Chin. Phys. Lett.* **27** 104701
[27] Li K and Zhong C W 2015 *Chin. Phys. B* **24** 050501
[28] Song B W, Ren F, Hu H B and Huang Q G 2015 *Chin. Phys. B* **24** 014703
[29] Zhang Y, Pan G and Huang Q G 2015 *Acta Phys. Sin.* **64** 184702 (in Chinese)
[30] Ladd A J C, Colvin M E and Frenkei D 1988 *Phys. Rev. Lett.* **60** 975
[31] Ladd A J C 1994 *J. Fluid Mech.* **271** 285
[32] Ladd A J C 1994 *J. Fluid Mech.* **271** 311
[33] Aidun C K and Lu Y 1995 *J. Stat. Phys.* **81** 49
[34] Aidun C K, Lu Y and Ding E 1998 *J. Fluid Mech.* **373** 287
[35] Ding E and Aidun C K 2003 *J. Stat. Phys.* **112** 685
[36] Ramachandran S, Sunil Kumar P B and Pagonabarraga I 2006 *Eur. Phys. J. E* **20** 151
[37] Alarcón F and Pagonabarraga I 2013 *J. Mol. Liq.* **185** 56
[38] Chwang A T and Wu T Y T 1974 *J. Fluid Mech.* **63** 607
[39] Chwang A T and Wu T Y T 1975 *J. Fluid Mech.* **67** 787
[40] Chwang A T 1975 *J. Fluid Mech.* **72** 17
[41] Ku X K and Lin J Z 2009 *Phys. Scr.* **80** 025801
[42] Bhatnagar P L, Gross E P and Krook M 1954 *Phys. Rev.* **94** 511
[43] Chen H, Chen S and Matthaeus W H 1992 *Phys. Rev. A* **45** R5339
[44] Chen S and Doolen G D 1998 *Annu. Rev. Fluid Mech.* **30** 329
[45] Happel J and Brenner H 1965 *Low Reynolds Number Hydrodynamics*, 1st edn. (Hague: Martinus Nijhoff Publishers)
[46] Keller S R and Wu T Y 1977 *J. Fluid Mech.* **80** 259